

Article

In Vivo Preclinical Assessment of the VEGF Targeting Potential of the Newly Synthesized [⁵²Mn]Mn-DOTAGA-Bevacizumab Using Experimental Cervix Carcinoma Mouse Model

Csaba Csikos^{1,2}, Adrienn Vágner³, Gábor Nagy³, Ibolya Kálmán-Szabó¹, Judit P. Szabó¹, Minh Toan Ngo^{1,2}, Zoltán Szoboszlai³, Dezső Szikra¹, Zoárd Tibor Krasznai⁴, György Trencsényi^{1,2,*} and Ildikó Garai^{1,2,3,†}

¹ Division of Nuclear Medicine and Translational Imaging, Department of Medical Imaging, Faculty of Medicine, University of Debrecen, H-4032 Debrecen, Hungary

² Gyula Petrányi Doctoral School of Clinical Immunology and Allergology, Faculty of Medicine, University of Debrecen, H-4032 Debrecen, Hungary

³ Scanomed Ltd., H-4032 Debrecen, Hungary

⁴ Department of Obstetrics and Gynaecology, Faculty of Medicine, University of Debrecen, H-4032 Debrecen, Hungary

* Correspondence: trencsenyi.gyorgy@med.unideb.hu

† These authors contributed equally to this study.

Abstract: Among humanized monoclonal antibodies, bevacizumab specifically binds to vascular endothelial growth factor A (VEGF-A). VEGF-A is an overexpressed biomarker in cervix carcinoma and is involved in the development and maintenance of tumor-associated neo-angiogenesis. The non-invasive positron emission tomography using radiolabeled target-specific antibodies (immuno-PET) provides the longitudinal and quantitative assessment of tumor target expression. Due to antibodies having a long-circulating time, radioactive metal ions (e.g., ⁵²Mn) with longer half-lives are the best candidates for isotope conjugation. The aim of our preclinical study was to assess the biodistribution and tumor-targeting potential of ⁵²Mn-labeled DOTAGA-bevacizumab. The VEGF-A targeting potential of the new immuno-PET ligand was assessed by using the VEGF-A expressing KB-3-1 (human cervix carcinoma) tumor-bearing CB17 SCID mouse model and in vivo PET/MRI imaging. Due to the high and specific accumulation found in the subcutaneously located experimental cervix carcinoma tumors, [⁵²Mn]Mn-DOTAGA-bevacizumab is a promising PET probe for the detection of VEGF-A positive gynecological tumors, for patient selection, and monitoring the efficacy of therapies targeting angiogenesis.

Keywords: ⁵²Mn; bevacizumab; cervix carcinoma; positron emission tomography; VEGF



Citation: Csikos, C.; Vágner, A.; Nagy, G.; Kálmán-Szabó, I.; Szabó, J.P.; Ngo, M.T.; Szoboszlai, Z.; Szikra, D.; Krasznai, Z.T.; Trencsényi, G.; et al. In Vivo Preclinical Assessment of the VEGF Targeting Potential of the Newly Synthesized [⁵²Mn]Mn-DOTAGA-Bevacizumab Using Experimental Cervix Carcinoma Mouse Model. *Diagnostics* **2023**, *13*, 236. <https://doi.org/10.3390/diagnostics13020236>

Academic Editor: Zhen Cheng

Received: 24 November 2022

Revised: 19 December 2022

Accepted: 5 January 2023

Published: 8 January 2023



Copyright: © 2023 by the authors. Licensee MDPI, Basel, Switzerland. This article is an open access article distributed under the terms and conditions of the Creative Commons Attribution (CC BY) license (<https://creativecommons.org/licenses/by/4.0/>).

1. Introduction

Cervical carcinoma is the fourth most common gynecologic malignancy in women behind, breast, colorectal, and lung cancer. In 2018, more than 500,000 women were diagnosed worldwide with cervical cancer, and of this high number, unfortunately, we have lost more than 300,000 patients with an incidence of 13.1/100,000 [1,2]. Improving the overall five-year survival rate, which was only 66% between 2010 and 2016, is essential [3].

Tumor-associated angiogenesis is a great concern, and it can immensely contribute to the progression and mortality of the disease. One of the players in tumor angiogenesis is the vascular endothelial growth factor (VEGF) family [4]. Different subtypes of VEGF exist (VEGF-A, -B, -C, -D, -E, and PDGF) from which VEGF-A is responsible for blood vessel growth. Its physiological role is to contribute to embryological, reproductive, and bone angiogenesis. VEGF-A can be overexpressed by several types of malignant cells. After secretion, VEGF can bind to VEGF receptors (VEGFR) located on the surface of endothelial cells. VEGF-A has a higher affinity to tyrosine kinase receptors such as VEGFR-1 and VEGFR-2. Mainly through VEGFR-2, signaling pathways can become activated

(e.g., PI3K-Akt and PLC γ -PKC-MAPK pathways) that lead to both tumor growth and angiogenesis [5].

Bevacizumab, as an anti-VEGF antibody, is a widely used monoclonal antibody in the therapy of advanced cervical cancer [6]. It can block the proliferation and angiogenesis of cancer cells and, therefore, slow the progression of cervical carcinoma by binding to VEGF [7]. However, no biomarker has been developed that would be a useful modality to predict the effectiveness of bevacizumab therapy and monitor later-developed drug resistance.

Nuclear medicine plays an important role in diagnosing and staging malignancies and in treatment planning using ^{18}F -FDG PET/CT [8]. Molecular imaging has further potential through radiolabeling targeted therapeutic agents, such as bevacizumab (immuno-PET) [9]. Within the tools of nuclear medicine and molecular imaging, PET/CT and PET/MRI—as hybrid imaging techniques—make visual assessment possible; moreover, the appearance of each lesion can be described objectively using numerical parameters obtained from the images [10].

Monoclonal antibodies are promising candidates for molecular imaging, as they specifically bind to their target molecule, and their labeling with a radioactive isotope can be easily carried out. Antibodies have a long circulation time in the blood, and due to this property, radioactive metal ions with a long half-life are the most suitable for their radioisotope labeling; however, metal ions are not capable of direct binding to immunoglobulins, so the use of chelating agents is necessary [9]. It is difficult to find an isotope that forms a stable metal ion-chelator complex. Several isotopes (e.g., ^{89}Zr , ^{86}Y , ^{64}Cu , ^{111}In) conjugated with bevacizumab have been investigated, from which zirconium-89 (^{89}Zr) positron-emitting isotope seemed to be the most promising due to its ideal half-life ($t_{1/2} = 3.27$ days) [11]. A chelator suitable for the coordination sphere of ^{89}Zr , which can prevent its release from the complex leading to the accumulation of the isotope in the bones, has not been found so far [12]. According to this, the use of an isotope whose stable complex can be more easily produced would be a safer and better choice for patients. Manganese-52 (^{52}Mn) ($t_{1/2} = 5.59$ days) is a novel positron-emitting isotope, so there is not much literature about its use as a PET radiotracer, but a lot of data on the complex-forming properties of Mn^{2+} ion have been collected due to the use of manganese as an MRI contrast agent [13–16].

The aim of this preclinical study was to investigate the *in vivo* biodistribution and tumor targeting potential of the newly synthesized ^{52}Mn -labeled DOTAGA-bevacizumab PET probe in the VEGF-A positive cervix carcinoma tumor-bearing mouse model.

2. Materials and Methods

2.1. General

For the radioactivity measurements, a Perkin Elmer Wizard gamma counter and the MED Isomed 2010 dose calibrator were used. To confirm the success of the labeling reactions, a radio-HPLC was used with the Waters Acquity UPLC I-class system, connected to a radioactivity detector (Berthold LB513; Radchem Co. Ltd., Budapest, Hungary) with a 20 μL plastic scintillator (MX) cell.

2.2. Chemicals

Rotipuran Ultra H_2O (u.p. H_2O), 34% Rotipuran Ultra HCl (u.p. HCl), and Pufferan $\geq 99.5\%$ Cellpure HEPES were purchased from Carl Roth. Ultra-pure ammonium acetate (u.p. NH_4OAc) was bought from VWR. HPLC-MS grade ACN was provided by Scharlau. The Xbridge Premier Protein SEC column (250 \AA 2.5 μm , 4.6 \times 150 mm) was supplied by Waters.

2.3. Radiolabeling

Bevacizumab (Avastin $^{\text{®}}$; Roche Pharma AG, Grenzach-Wyhlen, Germany) was derivatized with a fivefold excess of 2,2',2''-(10-(1-carboxy-4-((4-isothiocyanatobenzyl)amino)-4-oxobutyl)-1,4,7,10-tetraazacyclododecane-1,4,7-triyl)triacetic acid (p-NCS-Bn-DOTA-GA;

Chematech) in NaHCO_3 buffer (pH 8.2) at room temperature. DOTAGA-bevacizumab was purified by ultrafiltration on an Amicon Ultra (Merck KGaA, Darmstadt, Germany), 0.5 mL, 30 kDa centrifugal filter (Millipore). Radiolabeling was implemented at pH 6 for 15 min at room temperature. The required pH value was adjusted by sodium-acetate (0.04 M) buffer and sodium hydroxy. The efficiency of radiolabeling was followed by Raytest miniGita Star radio-thin layer chromatography scanner. 3 μL of the reaction mixture was dropped onto a glass macrofibre chromatography paper impregnated with silica gel (iTLC-SG) strip and developed in 0.1 M sodium citrate solution. ^{52}Mn]Mn-DOTAGA-bevacizumab was remained near the start point ($R_f = 0.1\text{--}0.2$), whereas $^{52}\text{Mn}^{\text{II}}$ as citrate complex was eluted with the solvent front ($R_f = 0.8\text{--}1$). The ^{52}Mn]Mn-DOTAGA-bevacizumab product was used without further purification in experiments.

2.4. Determination of In Vitro Stability of ^{52}Mn]Mn-DOTAGA-Bevacizumab

^{52}Mn]Mn-DOTAGA-bevacizumab was diluted with fourfold excess of 0.01 M EDTA (pH 7.3), 0.01 M oxalic acid (pH 5.7), and mouse serum solution to investigate its stability. In the case of stability experiments against EDTA and oxalic acid, the reaction was carried out at 25 °C for 0.17, 1.5, 3, 21, and 47 h. In the case of stability investigation in mouse serum, the reaction mixture was incubated at 37 °C, and sampling was performed at 0.2, 4, 22, 47, 118, and 167 h, where samples were diluted fivefold with water before directly injected into UPLC. In each case, samples were analyzed on an Xbridge Premier Protein SEC 250 column (Waters) using an isocratic method with 0.45 mL/min flow rate, where the liquid phase was 100 mM ammonium acetate (pH 7.2) solution.

2.5. Cell Lines

Human KB-3-1 cervix carcinoma cell line [17] was obtained from Dr. Katalin Goda (University of Debrecen, Faculty of Medicine, Department of Biophysics and Cell Biology). For cell culturing, the Dulbecco's Modified Eagle's medium (DMEM, GIBCO Life Technologies Magyarország Ltd., Budapest, Hungary) was used supplemented with Fetal Bovine Serum (10%, heat-inactivated FBS from GIBCO, Life technologies Magyarország Ltd., Budapest, Hungary) and Antibiotic and Antimycotic solution (1%, Sigma-Aldrich, Merck KGaA, Darmstadt, Germany). KB-3-1 cells were maintained at standard culturing conditions (5% CO_2 and 37 °C). For subcutaneous tumor inoculation, cervix carcinoma cells were used at 80% confluency, and the cell viability was confirmed by the trypan blue exclusion test.

2.6. In Vivo Cervix Carcinoma Tumor Model

Immunodeficient CB17 SCID mice (12-week-old; female; $n = 35$) were housed under sterile conditions in individually ventilated cage system (IVC cages, Techniplast, Akro-nom Ltd., Budapest, Hungary) under standard conditions (25 ± 2 °C and $55 \pm 10\%$). A sterile semi-synthetic rodent diet (SDS VRF, Animalab Ltd., Budapest, Hungary) and sterile tap water were available ad libitum to all the experimental animals. Experimental animals were kept and treated in accordance with all the corresponding paragraphs of the Hungarian Ethical Laws and the regulations of the European Union (permission number: 16/2020/DEMÁB).

For the establishment of the KB-3-1 cervix carcinoma tumor model, experimental animals were anesthetized by 3% isoflurane (Forane, AbbVie, Budapest, Hungary; OGYI-T-1414/01), O_2 0.4 L/min and N_2O 1.2 L/min (Linde Healthcare, Budapest, Hungary; OGYI-T-20607 and OGYI-T-21090, respectively) using the Tec3 Isoflurane Vaporizer anesthesia device (Eickemeyer, Sunbury-on-Thames, Surrey, UK), then 5×10^6 KB-3-1 tumor cells in saline (150 μL 0.9% NaCl) were injected subcutaneously into the right shoulder area of the experimental animals. In vivo imaging and ex vivo biodistribution studies were carried out 11 ± 1 days after the implantation of KB-3-1 cancer cells at the tumor volume of approximately 75 mm^3 .

2.7. *In Vivo* PET/MRI Imaging

KB-3-1 cervix carcinoma tumor-bearing mice were anesthetized by 1.5% isoflurane, and for the anatomical localization of the investigated tissues, whole-body MRI scans (T1-weighted) were performed using the preclinical *nanoScan* PET/MRI system (Mediso Ltd., Budapest, Hungary). The 3D GRE EXT multi-FOV MRI parameters were set as follows: TR/TE 15/2 ms; phase: 100; FOV 60 mm; NEX 2. After MRI imaging, animals were injected intravenously with 9.43 ± 1.03 MBq of $^{52}\text{MnCl}_2$, [^{52}Mn]Mn-DOTAGA, or [^{52}Mn]Mn-DOTAGA-bevacizumab and dynamic PET scans were performed. The co-registered and reconstructed (3D-OSEM algorithm with Tera-Tomo reconstruction software, Mediso Ltd., Budapest, Hungary) decay-corrected PET images were analyzed by the InterView™ FUSION (Mediso Ltd., Budapest, Hungary) image analysis software. Volumes of Interest (ellipsoidal 3-dimensional VOIs) were manually drawn around the edge of the activity of the investigated tissues and organs by visual inspection. The accumulation of the ^{52}Mn -labeled probes was expressed in terms of standardized uptake values (SUVs).

2.8. Immunohistochemistry

For the detection of the VEGF-A expression of the subcutaneously growing KB-3-1 cervix carcinoma, xenografts cryosections (5 μm thick) were made from the tumors. Sections were dried, fixed (10 min at -20 °C in pre-cooled acetone), blocked (20 min with 1% BSA-PBS), and were further incubated at 24 °C with anti-human VEGF Alexa Fluor® 488-conjugated monoclonal antibody (IC2931G; Bio-Techne R&D Systems Ltd. Budapest, Hungary). For nuclear counterstaining DAPI, (MBD0020; DAPI ready-made solution with Antifade; Merck, Darmstadt, Germany) was used. For fluorescence imaging, the Zeiss LSM 510 confocal laser-scanning microscope was used.

2.9. Statistical Analysis

The statistical significance was assessed by the Student's t-test (two-tailed), two-way ANOVA, and Mann-Whitney U-test using the MedCalc software (MedCalc Software v18.5., Mariakerke, Belgium; <https://www.medcalc.org>, accessed on 17 December 2022). Quantitative data were presented as mean \pm SD, and the level of significance was set at $p < 0.05$.

3. Results

3.1. Radiolabeling and Characterization of [^{52}Mn]Mn-DOTAGA-Bevacizumab

The chemical purity of the DOTAGA-bevacizumab precursor was verified with an HPLC-UV-MS system. The DOTAGA/bevacizumab ratio was calculated based on the consumption of DOTAGA pSCN-Bn, during which the DOTAGA/bevacizumab ratio was 4.42 ± 0.26 . DOTAGA-bevacizumab was labeled with $^{52}\text{MnCl}_2$ (Figure 1) with a specific activity of 0.01 MBq/ μg . The final radiochemical yield (RCY) was $>90\%$, measured by thin-layer chromatography. The stability of [^{52}Mn]Mn-DOTAGA-bevacizumab was investigated in EDTA, oxalic acid solution, and mouse serum and assessed by size-exclusion chromatography. [^{52}Mn]Mn-DOTAGA-bevacizumab was stable against EDTA and oxalic acid, with only about a 5% decrease in radiochemical yield over 48 h (Figure 2A). The radiochemical yield of [^{52}Mn]Mn-DOTAGA-bevacizumab was above $>70\%$ for up to 7 days in mouse serum (Figure 2B).

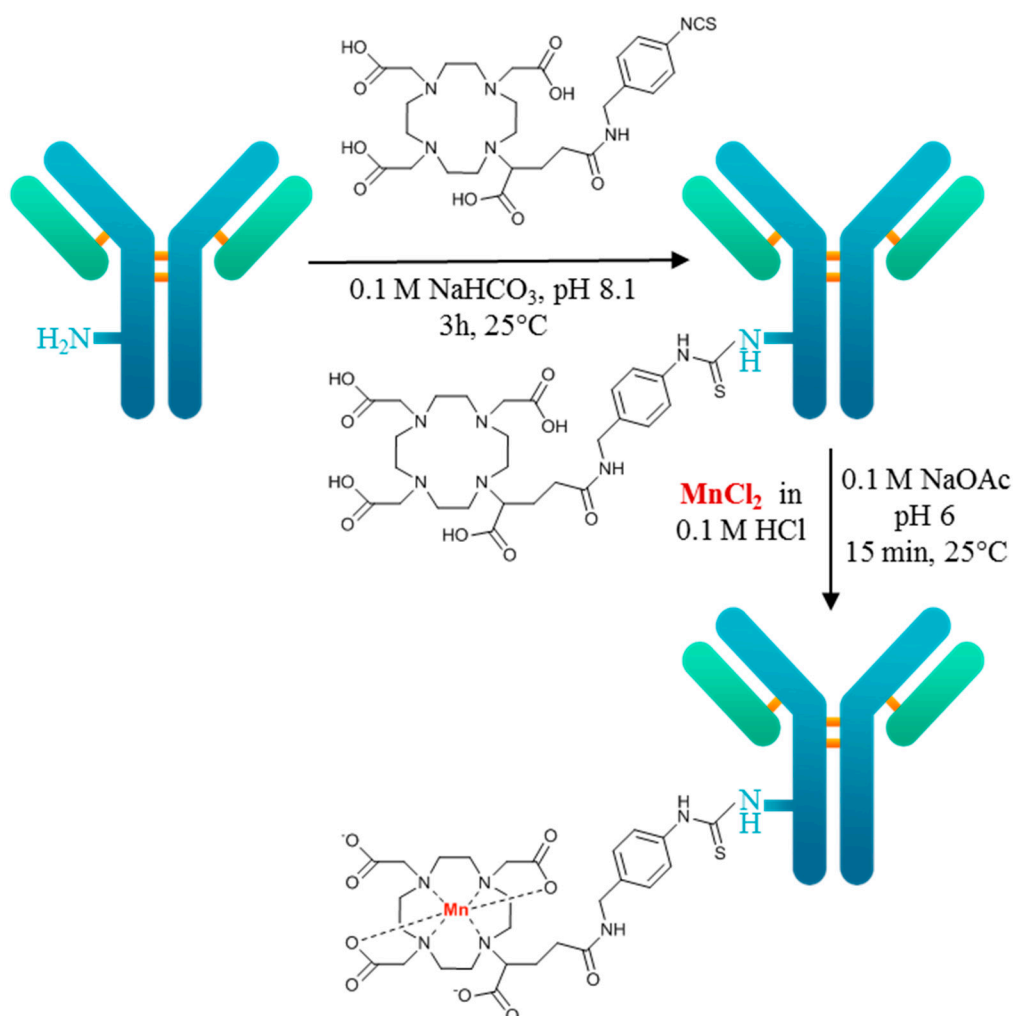


Figure 1. Scheme of the radiochemical synthesis of [⁵²Mn]Mn-DOTAGA-bevacizumab.

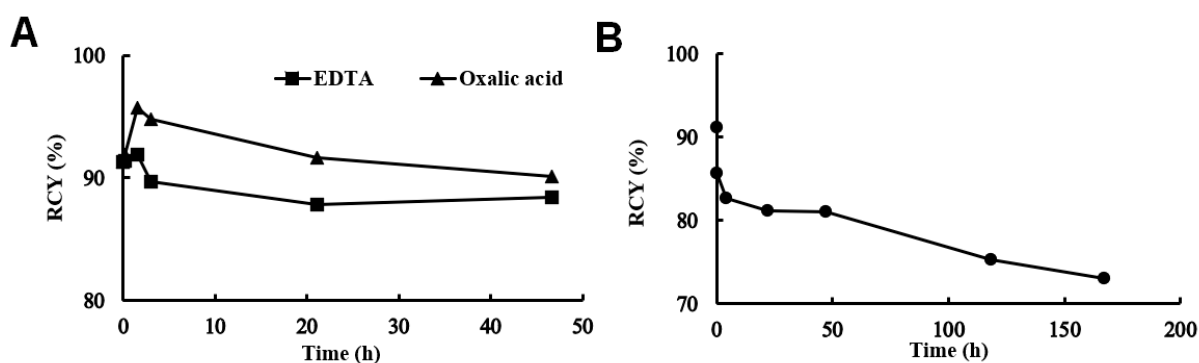


Figure 2. Stability of [⁵²Mn]Mn-DOTAGA-bevacizumab in EDTA and oxalic acid (A) and mouse serum (B).

3.2. Biodistribution and PET/MRI Imaging Studies

For the assessment of VEGF receptor specificity of [⁵²Mn]Mn-DOTAGA-bevacizumab, *in vivo* tissue distribution studies were executed by healthy and KB-3-1 tumor-bearing SCID mice. In the first experiments, for the confirmation that the newly synthesized [⁵²Mn]Mn-DOTAGA-bevacizumab probe is stable *in vivo*, the uptake values of the biodistribution were compared to that of ⁵²MnCl₂ (Figure 3) and [⁵²Mn]Mn-DOTAGA in healthy control mice (Figure 4). The SUV_{mean} values of the selected organs were assessed at seven different

time points (4 h, 1, 2, 3, 5, 7, and 10 days) after tracer injection. The qualitative PET image and the quantitative SUV data analysis showed that the accumulation of $^{52}\text{MnCl}_2$ in the liver and kidney cortex was initially remarkable; however, the $^{52}\text{MnCl}_2$ content in these organs decreased with time. The activity concentration of the pancreas and salivary glands also showed high values, which did not decrease as time progressed (Figure 3).

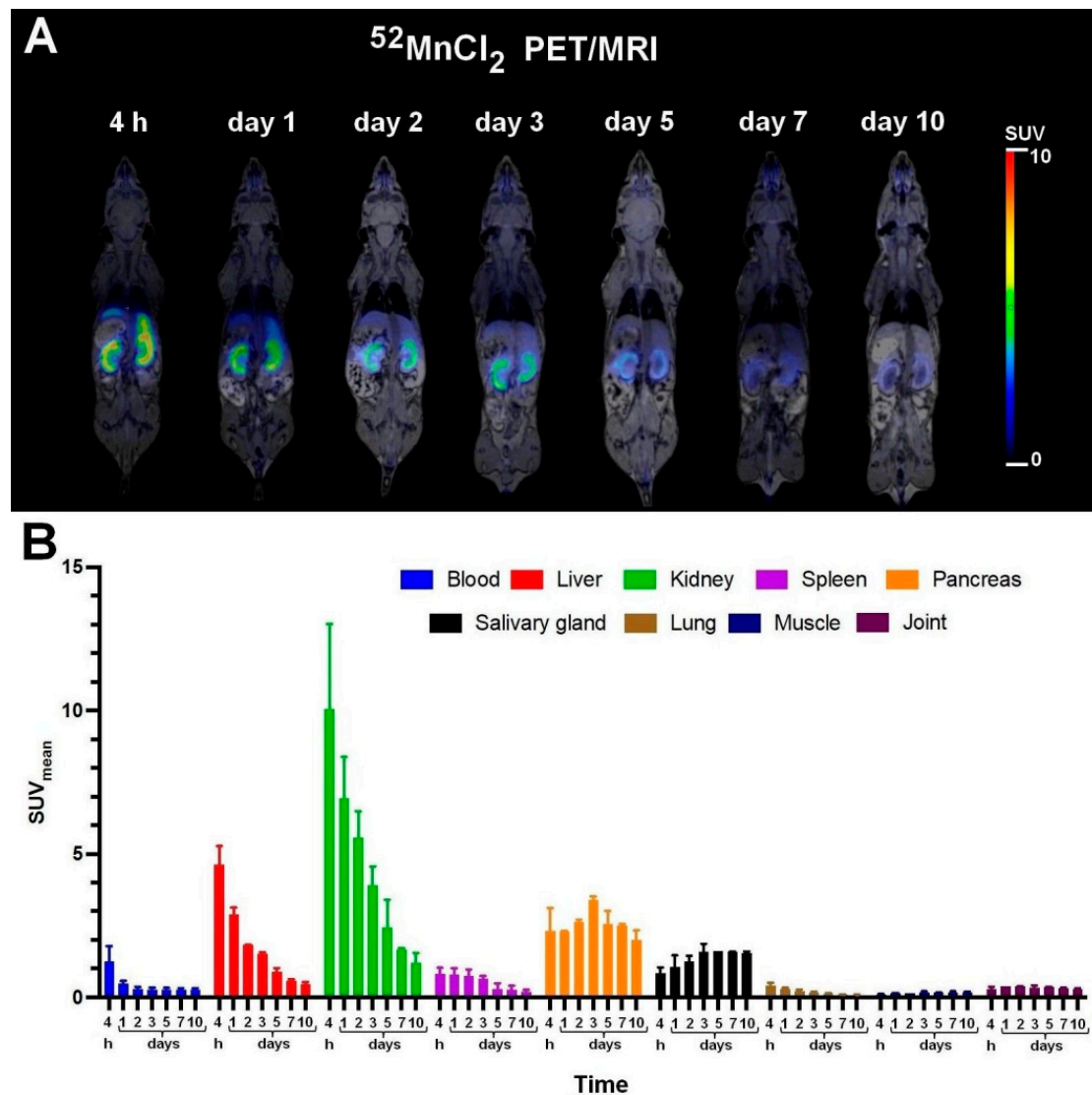


Figure 3. In vivo PET/MRI imaging of $^{52}\text{MnCl}_2$ biodistribution (A) and average time-activity changes (B) of the selected organs 4 h, 1, 2, 3, 5, 7, and 10 days after the intravenous injection of approximately 10 MBq of $^{52}\text{MnCl}_2$. SUV: standardized uptake value. Data are shown as mean \pm SD and obtained from $n = 5$ animals.

In the case of $[^{52}\text{Mn}]\text{Mn-DOTAGA}$, only the uptake of the lungs was prominent; however, this was also decreased rapidly, and $[^{52}\text{Mn}]\text{Mn-DOTAGA}$ showed very low uptake values in all of the other investigated organs due to the rapid clearance at the early time points (Figure 4). $[^{52}\text{Mn}]\text{Mn-DOTAGA-bevacizumab}$ showed elevated uptake in the blood, liver, kidney, spleen, and lung, although a continuous decrease in activity concentration was also observed in these organs till ten days post-injection (Figure 5). In summary, $[^{52}\text{Mn}]\text{Mn-DOTAGA}$ showed significantly lower uptake in all examined organs than that of the two other radiotracers.

The biodistribution and VEGF-A receptor specificity of the newly synthesized $[^{52}\text{Mn}]\text{Mn-DOTAGA-bevacizumab}$ was assessed by preclinical PET/MRI imaging using KB-3-1 tumor-

bearing mice. After the qualitative image analysis, it was found that the subcutaneously growing KB-3-1 cervix tumors were identifiable from 4 h after the tracer injection; moreover, an increasing accumulation of radiopharmaceuticals was observed as time progressed (Figure 5A). The quantitative SUV analysis of the PET images showed that the accumulation of [^{52}Mn]Mn-DOTAGA-bevacizumab was increasing until day 2–3 (SUV_{mean} : approx. 2) in the KB-3-1 tumors, then a decrease was observed with slow kinetics; however, the accumulation remained high for the rest of the investigated time points (SUV_{mean} : approx. 1.2 at day ten post-injection) (Figure 5B, insert). The presence of VEGF-A in the examined tumors was confirmed by immunohistochemical staining performed on day ten post injection of [^{52}Mn]Mn-DOTAGA-bevacizumab, and a strong expression was found in the membrane of the cancer cells (Figure 5C) confirming the target-specific property of the radiopharmaceutical.

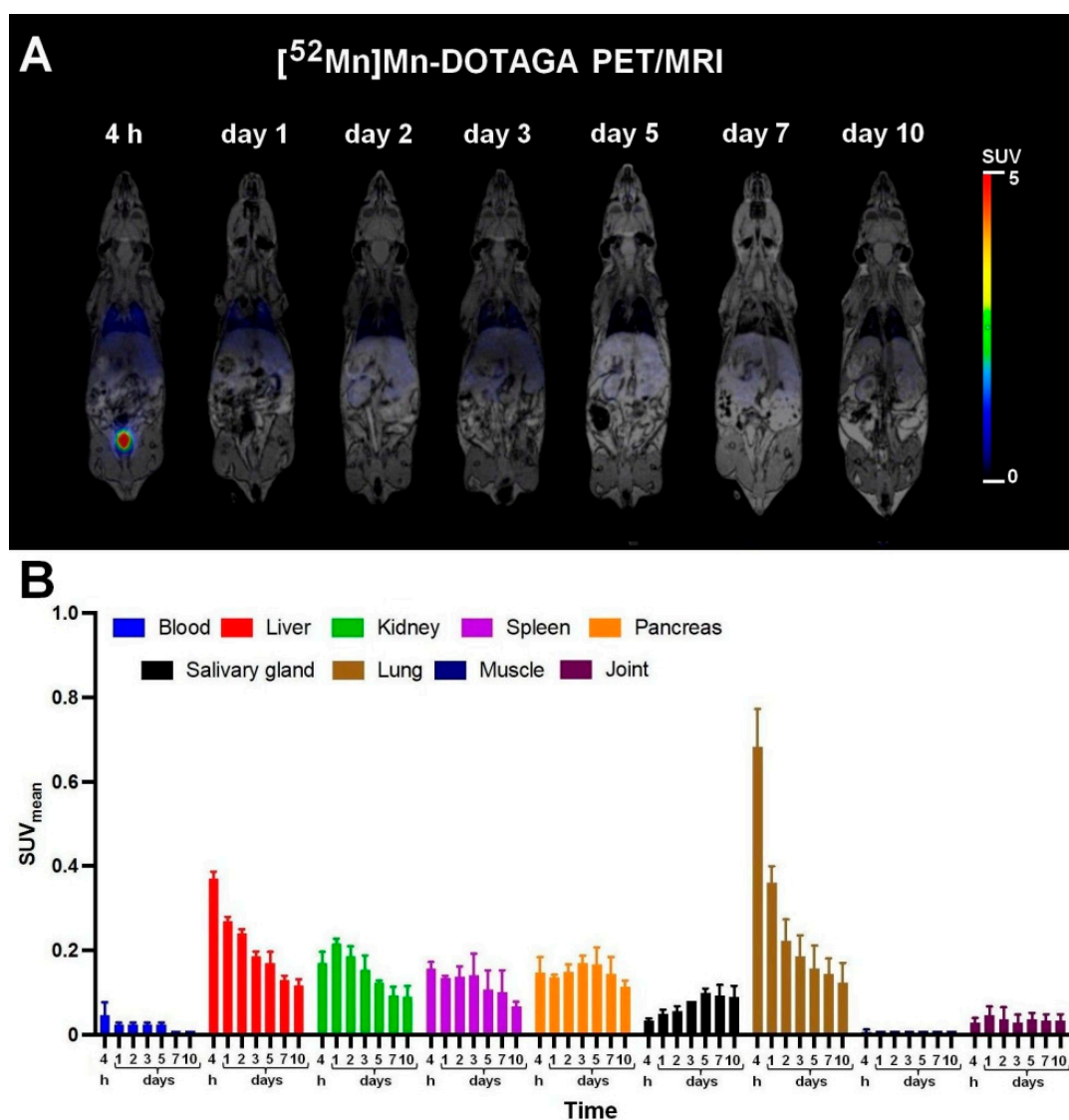


Figure 4. In vivo PET/MRI imaging of [^{52}Mn]Mn-DOTAGA biodistribution (A) and average time-activity changes (B) of the selected organs 4 h, 1, 2, 3, 5, 7, and 10 days after the intravenous injection of approximately 10 MBq of [^{52}Mn]Mn-DOTAGA. SUV: standardized uptake value. Data are shown as mean \pm SD and obtained from $n = 5$ animals.

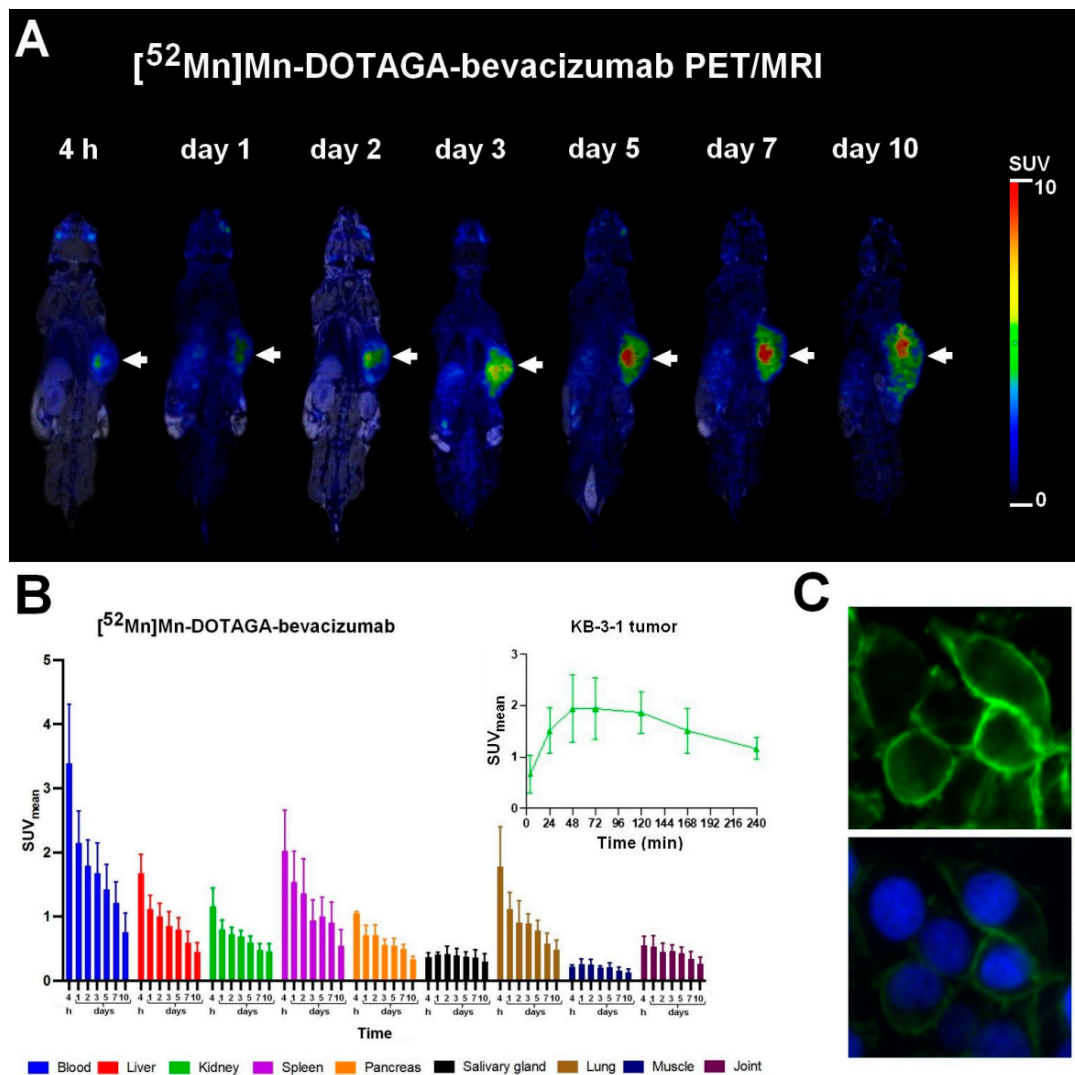


Figure 5. In vivo PET/MRI imaging of KB-3-1 cervix carcinoma tumor-bearing mice (A). Representative decay-corrected coronal PET/MRI images were obtained from 4 h to 10 days post injection of $[^{52}\text{Mn}]\text{Mn-DOTAGA-bevacizumab}$. White arrows: subcutaneously growing KB-3-1 cervix tumors. (B) The panel shows the biodistribution and the average time-activity curve (TAC) for the VEGF-A positive KB-3-1 tumors 4 h, 1, 2, 3, 5, 7, and 10 days after the intravenous injection of approximately 10 MBq of $[^{52}\text{Mn}]\text{Mn-DOTAGA-bevacizumab}$. SUV: standardized uptake value. Data are presented as mean \pm SD and obtained from $n = 5$ animals/time point. (C) panel demonstrates the VEGF-A positivity of subcutaneously growing KB-3-1 tumor by immunohistochemical study. Upper image: VEGF-A receptors (green color by Alexa-488 staining); lower image: VEGF-A receptors and nuclear counterstaining (blue color by DAPI staining).

Tumor-to-organ ratios ($\text{SUV}_{\text{mean tumor}}/\text{SUV}_{\text{mean organ}}$) were assessed by quantitative SUV data analysis of the PET images obtained from KB-3-1 tumorous mice after the i.v. injection of $[^{52}\text{Mn}]\text{Mn-DOTAGA-bevacizumab}$. It was generally observed that the ratio of the SUV_{mean} values started to plateau 2–3 days after ^{52}Mn -labeled DOTAGA-bevacizumab was injected, and these ratios remained high until the end of the study (ten days post-injection); however, in some cases (tumor-to-liver, -blood, -spleen) a slight increase was observed in the SUV_{mean} ratios from day three to day ten post-injection of $[^{52}\text{Mn}]\text{Mn-DOTAGA-bevacizumab}$ (Figure 6).

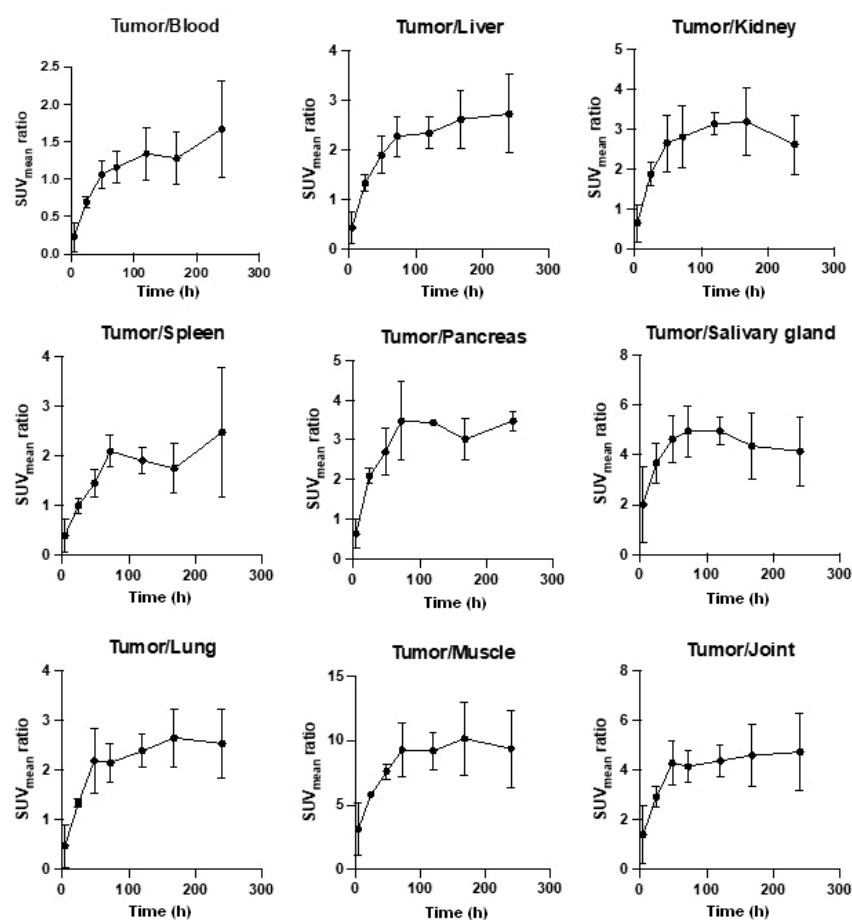


Figure 6. Quantitative assessment of KB-3-1 tumor-to-organ ratios in CB17 SCID mice after the i.v. injection of [^{52}Mn]Mn-DOTAGA-bevacizumab. SUV: standardized uptake value. Data are shown as mean \pm SD and obtained from $n = 5$ animals/time point.

4. Discussion

Among humanized monoclonal antibodies, bevacizumab specifically binds to vascular endothelial growth factor A (VEGF-A), which is an overexpressed biomarker in different tumor types and plays an important role in the development and maintenance of tumor-associated angiogenesis. The standard protocol for biomarker quantification is generally biopsy sampling and immunohistochemistry (IHC) or mRNA validation. Nevertheless, the evaluation of biomarker expression is influenced by the tumor heterogeneity and sampling errors. In addition, repetitive biopsies and histopathological confirmation are required to monitor treatment response, making clinical use challenging [18,19]. In contrast, the nanomolar sensitivity of the non-invasive positron emission tomography using radiolabeled target-specific monoclonal antibodies (immuno-PET) provides the longitudinal and quantitative assessment of tumor target expression [20,21].

In this present study, the VEGF-A targeting ability of the new immuno-PET probe was assessed by using the VEGF-A expressing KB-3-1 (human cervix carcinoma) tumor-bearing CB17 SCID mouse model and in vivo PET/MRI imaging. The new [^{52}Mn]Mn-DOTAGA-bevacizumab PET probe was synthesized with high radiochemical purity and appropriate stability properties (Figures 1 and 2). Similar stability data were also described by other authors (e.g., $^{99\text{m}}\text{Tc}$ -labeled BevMab-DTPA, ^{131}I -bevacizumab); however, they examined the stability in serum for 24 and 48 h, respectively, due to the difference in the half-life of the radionuclides used [22,23].

By the biodistribution studies, it has been found that the fastest clearance was seen with [^{52}Mn]Mn-DOTAGA through the kidney, and therefore, its activity was very low at all the investigated time points (Figure 4). $^{52}\text{MnCl}_2$ (Figure 3) and [^{52}Mn]Mn-DOTAGA-

bevacizumab needed longer time for excretion. $^{52}\text{Mn}^{2+}$ was excreted mainly via the kidneys, while the antibody stayed in the blood for a long time and showed relatively high uptake in the lung (Figure 5).

Bevacizumab is specific for the human VEGF and inhibits its biological activity [24]. It is also known that the presence and over-expression of VEGF in cervix carcinomas is an outstanding prognostic marker and is associated with poor patient survival [25,26]. Accordingly, we also found strong positivity for VEGF expression by immunohistochemical studies and found high and specific accumulation of [^{52}Mn]Mn-DOTAGA-bevacizumab in the VEGF-A positive KB-3-1 cervical cancer xenografts (Figure 5), however. In addition, an important parameter for the assessment of PET images is the radioactivity concentration of healthy organs and tissues compared to the tumor. These data also provide information on non-specific and off-target binding. The evaluation of these data is also important due to it was observed that bevacizumab binds with high affinity to, for example, brain receptors (dopamine, GABA, histamine), whereas the amounts of substances used in PET diagnostics do not cause a pharmacological effect or side-effect [24]. In this present study, the tumor-to-background ratios increased and reached a plateau 2–3 days after the administration of ^{52}Mn -labeled bevacizumab and remained high until the end of the study, indicating the specific accumulation and high binding affinity in the tumors (Figure 6).

From our observations, we can conclude that [^{52}Mn]Mn-DOTAGA-bevacizumab could be a useful tracer for patient selection to bevacizumab therapy, as well as monitoring the efficacy of the targeted therapy and later developed drug resistance. Numerous preclinical studies have been published using different isotopes for this purpose, including ^{116}Ho , ^{89}Zr , ^{111}In , ^{86}Y , and $^{99\text{m}}\text{Tc}$ [27–31]. Furthermore, several human clinical studies are known from the literature in which ^{89}Zr -labeled bevacizumab has outstanding tumor targeting and PET imaging ability [32–37]. However, the above-mentioned isotopes have shorter half-lives than ^{52}Mn . Since bevacizumab stays in the circulation for a long time, and tumor-to-background ratios remain elevated for several days, ^{52}Mn may potentially be a more ideal candidate to use for immunoPET imaging of anti-VEGF target drug than isotopes with shorter half-lives. Moreover, the favorable and well-described chelating properties of Mn^{2+} make it possible to use chelators that form stable complexes not only with ^{52}Mn but also with β^- and α emitting therapeutic isotopes like ^{177}Lu and ^{225}Ac [38,39]. This feature could lead to the use of bevacizumab as a theranostic agent as well.

5. Conclusions

In conclusion, due to high and specific accumulation observed in the subcutaneously growing KB-3-1 experimental cervix carcinoma tumors, [^{52}Mn]Mn-DOTAGA-bevacizumab is a promising radiopharmaceutical in the imaging of VEGF-A positive gynecological tumors, in patient selection, and monitoring the efficacy of therapies targeting angiogenesis.

Author Contributions: Conceptualization, I.G., G.N., A.V., Z.T.K. and G.T.; data curation, I.G.; investigation, C.C., G.N., A.V., J.P.S., I.K.-S. and D.S.; methodology, I.G., G.N., A.V., J.P.S., M.T.N., Z.S. and G.T.; validation, D.S. and G.N.; visualization, C.C., G.N., A.V. and G.T.; writing—original draft, C.C., G.N., A.V. and G.T.; writing—review & editing, I.G., D.S. and G.T. All authors have read and agreed to the published version of the manuscript.

Funding: This research work was conducted with the support of the National Academy of Scientist Education Program of the National Biomedical Foundation under the sponsorship of the Hungarian Ministry of Culture and Innovation (C.C. and G.T.) The published work was supported by the EFOP-3.6.3-VEKOP-16-2017-00009 fund of the European Union, by the NKFIH K119552 grant of the European Social Fund and National Research, Development, and Innovation Office, and by the Thematic Excellence Programme (TKP2020-NKA-04) of the Ministry for Innovation and Technology in Hungary. This research was also supported by the KDP-2021 program of the Ministry for Innovation and Technology from the source of the national research, development, and innovation fund (G.T. and I.K.-S.).

Institutional Review Board Statement: All animal experiments were carried out in accordance with the European Communities Council directives 86/609/EEC on the use of experimental animals and local legislation on the ethics of animal experiments. The animal protocols were evaluated and approved by Institutional Ethics Committee for Animal Experimentation of the University of Debrecen, Hungary (permission number: 16/2020/DEMÁB).

Informed Consent Statement: Not applicable.

Data Availability Statement: The dataset used and analyzed in the current study are available from the corresponding author on reasonable request.

Conflicts of Interest: The authors declare no conflict of interest.

Abbreviations

^{52}Mn	manganese-52 isotope
DOTAGA	2,2',2''-(10-(1-carboxy-4-((4-isothiocyanatobenzyl)amino)-4-oxobutyl)-1,4,7,10-tetraazacyclododecane-1,4,7-triyl)triacetic acid
PET	positron emission tomography
RCY	radiochemical yield
VEGF	vascular endothelial growth factor

References

- Buskwofie, A.; David-West, G.; Clare, C.A. A Review of Cervical Cancer: Incidence and Disparities. *J. Natl. Med. Assoc.* **2020**, *112*, 229–232. [CrossRef] [PubMed]
- Cervical Cancer Survival Rates. Cancer 5 Year Survival Rates. Available online: <https://www.cancer.org/cancer/cervical-cancer/detection-diagnosis-staging/survival.html> (accessed on 21 November 2022).
- Arbyn, M.; Weiderpass, E.; Bruni, L.; de Sanjosé, S.; Saraiya, M.; Ferlay, J.; Bray, F. Estimates of Incidence and Mortality of Cervical Cancer in 2018: A Worldwide Analysis. *Lancet Glob. Health* **2019**, *8*, 191–203. [CrossRef] [PubMed]
- Lugano, R.; Ramachandran, M.; Dimberg, A. Tumor Angiogenesis: Causes, Consequences, Challenges and Opportunities. *Cell. Mol. Life Sci.* **2019**, *77*, 1745–1770. [CrossRef]
- Shibuya, M. Vascular Endothelial Growth Factor (VEGF) and Its Receptor (VEGFR) Signaling in Angiogenesis: A Crucial Target for Anti- and Pro-Angiogenic Therapies. *Genes Cancer* **2011**, *2*, 1097–1105. [CrossRef]
- Burmeister, C.A.; Khan, S.F.; Schäfer, G.; Mbatani, N.; Adams, T.; Moodley, J.; Prince, S. Cervical Cancer Therapies: Current Challenges and Future Perspectives. *Tumour Virus Res.* **2022**, *13*, 200238. [CrossRef] [PubMed]
- Garcia, J.; Hurwitz, H.I.; Sandler, A.B.; Miles, D.; Coleman, R.L.; Deurloo, R.; Chinot, O.L. Bevacizumab (Avastin®) in Cancer Treatment: A Review of 15 Years of Clinical Experience and Future Outlook. *Cancer Treat. Rev.* **2020**, *86*, 102017. [CrossRef]
- Herrera, F.G.; Prior, J.O. The Role of PET/CT in Cervical Cancer. *Front. Oncol.* **2013**, *3*, 34. [PubMed]
- Chomet, M.; van Dongen, G.A.M.S.; Vugts, D.J. State of the Art in Radiolabeling of Antibodies with Common and Uncommon Radiometals for Preclinical and Clinical Immuno-PET. *Bioconjug. Chem.* **2021**, *32*, 1315–1330. [CrossRef]
- Hofmann, M.; Pichler, B.; Schölkopf, B.; Beyer, T. Towards Quantitative PET/MRI: A Review of MR-Based Attenuation Correction Techniques. *Eur. J. Nucl. Med. Mol. Imaging* **2008**, *36*, 93–104. [CrossRef]
- Taurone, S.; Galli, F.; Signore, A.; Agostinelli, E.; Dierckx, R.A.J.O.; Minni, A.; Pucci, M.; Artico, M. VEGF in Nuclear Medicine: Clinical Application in Cancer and Future Perspectives (Review). *Int. J. Oncol.* **2016**, *49*, 437–447. [CrossRef]
- Raavé, R.; Sandker, G.; Adumeau, P.; Jacobsen, C.B.; Mangin, F.; Meyer, M.; Moreau, M.; Bernhard, C.; Da Costa, L.; Dubois, A.; et al. Direct Comparison of the in Vitro and in Vivo Stability of DFO, DFO* and DFOcyclo* for ^{89}Zr -ImmunoPET. *Eur. J. Nucl. Med. Mol. Imaging* **2019**, *46*, 1966–1977. [CrossRef] [PubMed]
- Csupász, T.; Szücs, D.; Kálmán, F.K.; Hollóczki, O.; Fekete, A.; Szikra, D.; Tóth, É.; Tóth, I.; Tircsó, G. A New Oxygen Containing Pyclyen-Type Ligand as a Manganese(II) Binder for MRI and ^{52}Mn PET Applications: Equilibrium, Kinetic, Relaxometric, Structural and Radiochemical Studies. *Molecules* **2022**, *27*, 371. [CrossRef] [PubMed]
- Pan, D.; Schmieder, A.H.; Wickline, S.A.; Lanza, G.M. Manganese-Based MRI Contrast Agents: Past, Present, and Future. *Tetrahedron* **2011**, *67*, 8431–8444. [CrossRef] [PubMed]
- Devreux, M.; Henoumont, C.; Dioury, F.; Boutry, S.; Vacher, O.; Elst, L.V.; Port, M.; Muller, R.N.; Sandre, O.; Laurent, S. Mn^{2+} Complexes with Pyclyen-Based Derivatives as Contrast Agents for Magnetic Resonance Imaging: Synthesis and Relaxometry Characterization. *Inorg. Chem.* **2021**, *60*, 3604–3619. [CrossRef]
- Gale, E.M.; Atanasova, I.P.; Blasi, F.; Ay, I.; Caravan, P. A Manganese Alternative to Gadolinium for MRI Contrast. *J. Am. Chem. Soc.* **2015**, *137*, 15548–15557. [CrossRef]
- Krasznai, Z.T.; Trencsényi, G.; Krasznai, Z.; Mikecz, P.; Nizsalóczki, E.; Szalóki, G.; Szabó, J.P.; Balkay, L.; Márián, T.; Goda, K. ^{18}F FDG a PET Tumor Diagnostic Tracer Is Not a Substrate of the ABC Transporter P-Glycoprotein. *Eur. J. Pharm. Sci.* **2014**, *64*, 1–8. [CrossRef]

18. Yun, J.W.; Lee, S.; Ryu, D.; Park, S.; Park, W.Y.; Joung, J.G.; Jeong, J. Biomarkers Associated with Tumor Heterogeneity in Prostate Cancer. *Transl. Oncol.* **2019**, *12*, 43–48. [[CrossRef](#)]
19. Volkova, L.V.; Pashov, A.I.; Omelchuk, N.N. Cervical Carcinoma: Oncobiology and Biomarkers. *Int. J. Mol. Sci.* **2021**, *22*, 12571. [[CrossRef](#)]
20. Lugat, A.; Bailly, C.; Chérel, M.; Rousseau, C.; Kraeber-Bodéré, F.; Bodet-Milin, C.; Bourgeois, M. Immuno-PET: Design Options and Clinical Proof-of-Concept. *Front. Med.* **2022**, *9*, 1026083. [[CrossRef](#)]
21. Dewulf, J.; Adhikari, K.; Vangestel, C.; Wyngaert, T.V.D.; Elvas, F. Development of Antibody Immuno-PET/SPECT Radiopharmaceuticals for Imaging of Oncological Disorders—An Update. *Cancers* **2020**, *12*, 1868. [[CrossRef](#)]
22. Demir, I.; Muftuler, F.Z.B.; Unak, P.; Acar, C. In Vivo Investigation of Radiolabeled Bevacizumab in Healthy Rat Tissues. *Braz. Arch. Biol. Technol.* **2011**, *54*, 73–79. [[CrossRef](#)]
23. Ashrafi, S.A.; Hosseinimehr, S.J.; Varmira, K.; Abedi, S.M. Radioimmunotherapy with ¹³¹I-Bevacizumab as a Specific Molecule for Cells with Overexpression of the Vascular Endothelial Growth Factor. *Cancer Biother. Radiopharm.* **2012**, *27*, 420–425. [[CrossRef](#)]
24. Mukherjee, S.; Chatterjee, G.; Ghosh, M.; Das, B.; Majumder, D. Efficacy and Toxicity Assessment of Different Antibody Based Antiangiogenic Drugs by Computational Docking Method. *Adv. Bioinform.* **2016**, *2016*, 7053712. [[CrossRef](#)]
25. Yoshida, K.; Suzuki, S.; Sakata, J.; Utsumi, F.; Niimi, K.; Yoshikawa, N.; Nishino, K.; Shibata, K.; Kikkawa, F.; Kajiyama, H. The Upregulated Expression of Vascular Endothelial Growth Factor in Surgically Treated Patients with Recurrent/Radioresistant Cervical Cancer of the Uterus. *Oncol. Lett.* **2018**, *16*, 515–521. [[CrossRef](#)] [[PubMed](#)]
26. Zhang, J.; Liu, J.; Zhu, C.; He, J.; Chen, J.; Liang, Y.; Yang, F.; Wu, X.; Ma, X. Prognostic Role of Vascular Endothelial Growth Factor in Cervical Cancer: A Meta-Analysis. *Oncotarget* **2017**, *8*, 24797–24803. [[CrossRef](#)] [[PubMed](#)]
27. Khorami-Moghadam, A.; Bolouri, B.; Jalilian, A.R.; Bahrami-Samani, N.M.A.; Mazidi, S.M.; Alirezapour, B. Preclinical Evaluation of Holmium-166 Labeled Anti-VEGF-A(Bevacizumab). *J. Label. Comp. Radiopharm.* **2013**, *56*, 365–369. [[CrossRef](#)] [[PubMed](#)]
28. Nagengast, W.B.; de Vries, E.G.; Hospers, G.A.; Mulder, N.H.; de Jong, J.R.; Hollema, H.; Brouwers, A.H.; van Dongen, G.A.; Perk, L.R.; Lub-de Hooge, M.N. In Vivo VEGF Imaging with Radiolabeled Bevacizumab in a Human Ovarian Tumor Xenograft. *J. Nucl. Med.* **2007**, *48*, 1313–1319. [[CrossRef](#)]
29. Stollman, T.H.; Scheer, M.G.W.; Leenders, W.P.J.; Verrijp, K.C.N.; Soede, A.C.; Oyen, W.J.G.; Ruers, T.J.M.; Boerman, O.C. Specific Imaging of VEGF-A Expression with Radiolabeled Anti-VEGF Monoclonal Antibody. *Int. J. Cancer* **2008**, *122*, 2310–2314. [[CrossRef](#)]
30. Nayak, T.K.; Garmestani, K.; Baidoo, K.E.; Milenic, D.E.; Brechbiel, M.W. PET Imaging of Tumor Angiogenesis in Mice with VEGF-A-Targeted 86Y-CHX-A'-DTPA-Bevacizumab. *Int. J. Cancer* **2010**, *128*, 920–926. [[CrossRef](#)]
31. Camacho, X.; García, M.F.; Calzada, V.; Fernández, M.; Chabalgoity, J.A.; Moreno, M.; Barbosa de Aguiar, R.; Alonso, O.; Gambini, J.P.; Chammas, R.; et al. [^{99m}Tc(CO)₃]-Radiolabeled Bevacizumab: In Vitro and in Vivo Evaluation in a Melanoma Model. *Oncology* **2013**, *84*, 200–209. [[CrossRef](#)]
32. Gaykema, S.B.M.; Brouwers, A.H.; Lub-de Hooge, M.N.; Pleijhuis, R.G.; Timmer-Bosscha, H.; Pot, L.; van Dam, G.M.; van der Meulen, S.B.; de Jong, J.R.; Bart, J.; et al. ⁸⁹Zr-Bevacizumab PET Imaging in Primary Breast Cancer. *J. Nucl. Med.* **2013**, *54*, 1014–1018. [[CrossRef](#)]
33. Menke-van der Houven van Oordt, C.W.; McGeoch, A.; Bergstrom, M.; McSherry, I.; Smith, D.A.; Cleveland, M.; Al-Azzam, W.; Chen, L.; Verheul, H.; Hoekstra, O.S.; et al. Immuno-PET Imaging to Assess Target Engagement: Experience from ⁸⁹Zr-Anti-HER3 MAbs (GSK2849330) in Patients with Solid Tumors. *J. Nucl. Med.* **2019**, *60*, 902–909. [[CrossRef](#)] [[PubMed](#)]
34. Jansen, M.H.; Veldhuijzen van Zanten, S.E.M.; van Vuurden, D.G.; Huisman, M.C.; Vugts, D.J.; Hoekstra, O.S.; van Dongen, G.A.; Kaspers, G.J.L. Molecular Drug Imaging: ⁸⁹Zr-Bevacizumab PET in Children with Diffuse Intrinsic Pontine Glioma. *J. Nucl. Med.* **2016**, *58*, 711–716. [[CrossRef](#)]
35. Gaykema, S.B.M.; Schröder, C.P.; Vitfell-Rasmussen, J.; Chua, S.; Oude Munnink, T.H.; Brouwers, A.H.; Bongaerts, A.H.H.; Akimov, M.; Fernandez-Ibarra, C.; Lub-de Hooge, M.N.; et al. ⁸⁹Zr-Trastuzumab and ⁸⁹Zr-Bevacizumab PET to Evaluate the Effect of the HSP90 Inhibitor NVP-AUY922 in Metastatic Breast Cancer Patients. *Clin. Cancer Res.* **2014**, *20*, 3945–3954. [[CrossRef](#)] [[PubMed](#)]
36. Hegi-Johnson, F.; Rudd, S.E.; Wichmann, C.; Akhurst, T.; Roselt, P.; Trinh, J.; John, T.; Devereux, L.; Donnelly, P.S.; Hicks, R.; et al. ImmunoPET: IMaging of Cancer ImMUNOtherapy Targets with Positron Emission Tomography: A Phase 0/1 Study Characterising PD-L1 with ⁸⁹Zr-Durvalumab (MEDI4736) PET/CT in Stage III NSCLC Patients Receiving Chemoradiation Study Protocol. *BMJ Open* **2022**, *12*, e056708. [[CrossRef](#)] [[PubMed](#)]
37. Jauw, Y.W.S.; Huisman, M.C.; Nayak, T.K.; Vugts, D.J.; Christen, R.; Naegelen, V.M.; Ruettinger, D.; Heil, F.; Lammertsma, A.A.; Verheul, H.M.W.; et al. Assessment of Target-Mediated Uptake with Immuno-PET: Analysis of a Phase I Clinical Trial with an Anti-CD44 Antibody. *EJNMMI Res.* **2018**, *8*, 6. [[CrossRef](#)] [[PubMed](#)]
38. Wojdowska, W.; Karczmarczyk, U.; Balog, L.; Sawicka, A.; Pöstényi, Z.; Kovács-Haász, V.; Polyák, A.; Laszuk, E.; Mikołajczak, R.; Garnuszek, P. Impact of DOTA-Chelators on the Antitumor Activity of ¹⁷⁷Lu-DOTA-Rituximab Preparations in Lymphoma Tumor-Bearing Mice. *Cancer Biother. Radiopharm.* **2020**, *35*, 558–562. [[CrossRef](#)]
39. Thiele, N.A.; Wilson, J.J. Actinium-225 for Targeted α Therapy: Coordination Chemistry and Current Chelation Approaches. *Cancer Biother. Radiopharm.* **2018**, *33*, 336–348. [[CrossRef](#)]

Disclaimer/Publisher's Note: The statements, opinions and data contained in all publications are solely those of the individual author(s) and contributor(s) and not of MDPI and/or the editor(s). MDPI and/or the editor(s) disclaim responsibility for any injury to people or property resulting from any ideas, methods, instructions or products referred to in the content.